Micro-statistical modeling of an imperfect interface in a piezoelectric bimaterial under inplane static deformations

Xue Wang, Whye-Teong Ang* and Hui Fan
School of Mechanical and Aerospace Engineering
Nanyang Technological University

Abstract

A micro-statistical model is proposed for investigating the effective properties of a micro-damaged interface between a piezoelectric layer and a piezoelectric half-space under inplane electroelastostatic deformations. The interface is modeled as damaged by periodic arrays of micro-cracks. The lengths and the positions of the micro-cracks on a period interval of the interface are randomly generated. The conditions on the interfacial micro-cracks are formulated in terms of hypersingular integro-differential equations with the displacement and electrical potential jumps across the interface being unknown functions to be determined. To gain new useful physical insights into the behaviors of the imperfect interface, the influences of the material constants, the width of the layer and the crack densities of the interface on the effective properties of the interface are examined in details.

Keywords: Micro-statistical model, weak interface, piezoelectric materials, thin film, hypersingular integro-differential equations.

This is a preprint of the article in: Applied Mathematical Modelling 50 (2017) 695-714.

* Author for correspondence (W. T. Ang)
E-mail: mwtang@ntu.edu.sg
http://www.ntu.edu.sg/home/mwtang/

1 Introduction

For a mathematically more tractable analysis of layered materials having microscopically damaged interfaces, the interfaces may be simplified as ones with effective properties. Such an interface between two elastic materials denoted by 1 and 2 is modeled as a continuous distribution of springs with interfacial conditions given by

$$\underline{\underline{\boldsymbol{\sigma}}}^{(1)} \cdot \underline{\mathbf{n}} = \underline{\underline{\boldsymbol{\sigma}}}^{(2)} \cdot \underline{\mathbf{n}} = \underline{\underline{\mathbf{k}}} \cdot (\underline{\mathbf{u}}^{(1)} - \underline{\mathbf{u}}^{(2)}) \quad \text{on } \Gamma, \tag{1}$$

where Γ denotes the spring-like interface between the two elastic materials, $\underline{\mathbf{n}}$ is the unit normal vector to Γ pointing into material 1, $\underline{\mathbf{u}}^{(i)}$ and $\underline{\underline{\boldsymbol{\sigma}}}^{(i)}$ are respectively the displacement and the stress in material i and the second rank tensor $\underline{\underline{\mathbf{k}}}$ characterizes the effective stiffness of Γ. For works on interfaces described by the interfacial conditions in (1), one may refer to Benveniste and Miloh [5], Fan and Sze [7], Hashin [9] and Jones and Whittier [10].

As piezoelectric composites play an increasingly important role in engineering applications (Park el al. [15, 16] and Trolier-McKinstry and Muralt [21]), researchers have shown interest in the analyses of imperfect interfaces between piezoelectric materials. The interfacial conditions in (1) may be generalized to analyze weak interfaces between piezoelectric materials, as in Fan et al. [8] and Li and Lee [12]. In general, the interface between piezoelectric materials may be damaged both mechanically and electrically (Li et al. [14]), that is, not only the displacement is discontinuous across the weak interface, but the electric potential is also discontinuous. More specifically, for an interface Γ between two piezoelectric materials, the interfacial conditions in (1) may be generalized to

$$\left.\begin{array}{l} \underline{\underline{\boldsymbol{\sigma}}}^{(1)} \cdot \underline{\mathbf{n}} = \underline{\underline{\boldsymbol{\sigma}}}^{(2)} \cdot \underline{\mathbf{n}} = \underline{\underline{\mathbf{k}}} \cdot (\underline{\mathbf{u}}^{(1)} - \underline{\mathbf{u}}^{(2)}) + \underline{\mathbf{b}}\,(\phi^{(1)} - \phi^{(2)}) \\ \underline{\mathbf{D}}^{(1)} \cdot \underline{\mathbf{n}} = \underline{\mathbf{D}}^{(2)} \cdot \underline{\mathbf{n}} = \underline{\mathbf{c}} \cdot (\underline{\mathbf{u}}^{(1)} - \underline{\mathbf{u}}^{(2)}) + w(\phi^{(1)} - \phi^{(2)}) \end{array}\right\} \text{ on } \Gamma, \tag{2}$$

where $\phi^{(i)}$ and $\underline{\mathbf{D}}^{(i)}$ are respectively the electrical potential and the electrical displacement in material i and the scalar w, the vectors $\underline{\mathbf{b}}$ and $\underline{\mathbf{c}}$ and the second rank tensor $\underline{\underline{\mathbf{k}}}$ are tensorial quantities characterizing the effective properties of Γ.

Most existing research works on weak imperfect interfaces between piezoelectric materials decouple the elastic displacement and electrical potential jumps in the interfacial conditions in (2), that is, the assumption that $\underline{\mathbf{b}} = \underline{\mathbf{0}}$ and $\underline{\mathbf{c}} = \underline{\mathbf{0}}$ is made. Examples of papers making such an assumption include Chen and Lee [6], Kuo [11], Shodja et al. [18, 19], Sun et al. [20] and Zhou et al. [28]. Relatively few papers, such as Li et al. [13, 14] and Shi et al. [17], consider the coupling between the mechanical and electrical imperfections in the spring-like interface. The validity of the assumption that $\underline{\mathbf{b}} = \underline{\mathbf{0}}$ and $\underline{\mathbf{c}} = \underline{\mathbf{0}}$ has not been examined in detail in the literature. A clearer idea on this can be obtained by taking into consideration the micro details of the interface. A micro-model of the interface can be developed for estimating $\underline{\underline{\mathbf{k}}}$, $\underline{\mathbf{b}}$, $\underline{\mathbf{c}}$ and w. Such a model is used in Ang et al. [2] to analyze the effective properties of micro-damaged interfaces under antiplane electroelastostatic deformations.

In the present paper, we study the effective behaviors of the interface between a piezoelectric layer and a piezoelectric half-space under inplane deformations. It (the interface) is modeled as containing periodically repeated micro-cracks, which are taken to be either electrically permeable or electrically impermeable. As in the analyses of Wang et al. [22, 23, 24, 25] for weak interfaces between elastic materials, a statistical approach is adopted here to generate randomly the lengths and positions of the micro-cracks within a period interval of the interface. The conditions on the micro-cracks are formulated in terms of the hypersingular integro-differential equations, where both the displacement jumps and the electrical potential jumps across the

interface appear as the unknown functions to be determined. Once the hypersingular integro-differential equations are solved numerically, the effective properties of the interface may be readily calculated. For specific cases, the influences of the material constants, the thickness of the layer and the crack densities of the interface on the effective properties of the interface are examined in detail. From the results, we gain new useful physical insights into the effective behaviors of the imperfect interface between the piezoelectric layer and the piezoelectric half-space under inplane electroelastostatic deformations.

2 The problem

With reference to a Cartesian coordinate system $Ox_1x_2x_3$, consider an infinitely long piezoelectric layer bonded to a piezoelectric half-space. The layer and the half-space occupy respectively the regions $0 < x_2 < h$ and $x_2 < 0$. The interface $x_2 = 0$ between the layer and the half-space is damaged by a periodic array of micro-cracks. The layer and the half-space are assumed to be perfectly bonded on the uncracked parts of the interface.

A period interval of the interface contains an arbitrary number M of arbitrarily positioned micro-cracks of possibly different lengths. More specifically, the tips of the M micro-cracks in the region $0 < x_1 < L$ are taken to be $(a^{(m)}, 0)$ and $(b^{(m)}, 0)$ $(m = 1, 2, \ldots, M)$, where $a^{(m)}$ and $b^{(m)}$ satisfy $0 < a^{(1)} < b^{(1)} < a^{(2)} < b^{(2)} < \cdots < a^{(M)} < b^{(M)} < L$. The remaining parts of the interface are periodic replicas of the region $0 < x_1 < L$. Specifically, the tips of the micro-cracks on the remaining part of the interface are given by $a^{(k)} + nL < x_1 < b^{(k)} + nL$, for $k = 1, 2, \cdots, M$ and $n = \pm 1, \pm 2, \cdots$. Refer to Figure 1 for a geometrical sketch of the piezoelectric bimaterial for $M = 3$.

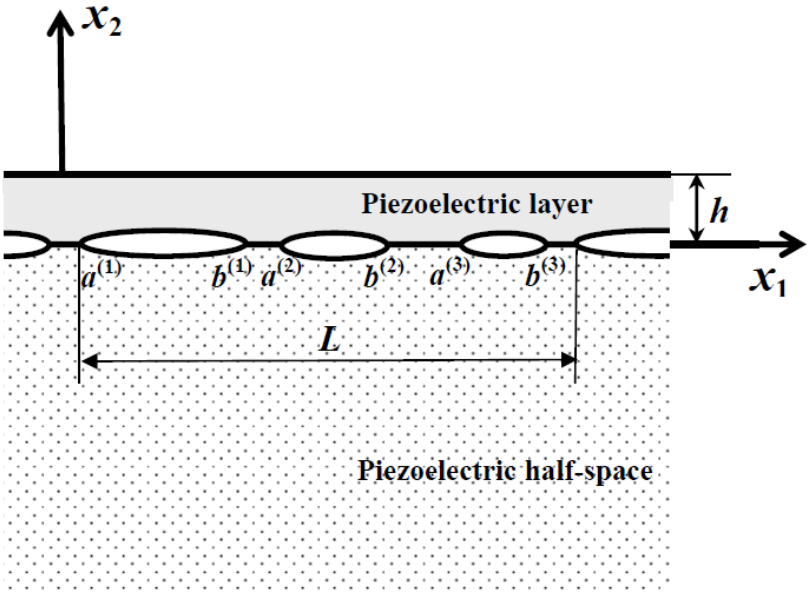

Figure 1. A geometrical sketch of the piezoelectric bimaterial for $M = 3$.

The bimaterial is subject to an inplane electroelastostatic deformation such that the Cartesian elastic displacements u_i. elastic stresses σ_{ij}, electrical potential ϕ and electrical displacements D_i are functions of only x_1 and x_2. The micro-cracks are assumed to open up and become traction-free under the electroelastostatic deformation.

If the micro-cracked interface between the piezoelectric layer and the piezoelectric half-space is simplified as a homogeneous interface with effective properties, the problem of interest here is to estimate the constant coefficients describing the effective properties of the interface.

If all the micro-cracks are electrically impermeable then the effective interface is electrically impermeable and is described by (2) which can be rewritten

in Cartesian coordinates as

$$\left.\begin{array}{c}\sigma_{i2}(x_1,0^+)=\sigma_{i2}(x_1,0^-)=k_{ij}^{(\mathrm{imp})}\Delta u_j(x_1)+b_i\Delta\phi(x_1)\\ D_2(x_1,0^+)=D_2(x_1,0^-)=c_i\Delta u_i(x_1)+w\Delta\phi(x_1)\end{array}\right\}\ \text{for}\ -\infty<x_1<\infty, \tag{3}$$

and the constant coefficients $k_{ij}^{(\mathrm{imp})}$, b_i, c_i and w are effective properties to be estimated. Note that $\Delta u_i(x_1) = u_i(x_1,0^+) - u_i(x_1,0^-)$ and $\Delta\phi(x_1) = \phi(x_1,0^+) - \phi(x_1,0^-)$ are respectively the displacement and electric potential jumps across the effective interface and the Einsteinian convention of summing over a repeated index is assumed for Latin subscripts running from 1 to 2.

On the other hand, if all the micro-cracks are electrically permeable, the electric potential is continuous on the electrically permeable effective interface and the interfacial conditions in (3) is modified to become

$$\left.\begin{array}{c}\sigma_{i2}(x_1,0^+)=\sigma_{i2}(x_1,0^-)=k_{ij}^{(\mathrm{per})}\Delta u_j(x_1)\\ D_2(x_1,0^+)=D_2(x_1,0^-)\\ \Delta\phi(x_1)=0\end{array}\right\}\ \text{for}\ -\infty<x_1<\infty, \tag{4}$$

and $k_{ij}^{(\mathrm{per})}$ are the effective stiffness coefficients to be estimated.

3 Formulation and computation

In this section, we present the basic equations of electroelastostatics to formulate the problem stated in Section 2 as a boundary value problem, express the boundary value problem in terms of a system of hypersingular integro-differential equations and outline a computational procedure for estimating the effective properties of the micro-damaged interface under electroelastostatic deformations.

3.1 Boundary value problem

The piezoelectric bimaterial in Section 2 undergoes the inplane deformations and the electrical poling is along the x_2 direction. The relevant Cartesian components of the inplane stresses σ_{ij} and the electric displacement D_j are related to one another by

$$\begin{aligned}
\sigma_{11} &= c_{11}(x_2)\frac{\partial u_1}{\partial x_1} + c_{12}(x_2)\frac{\partial u_2}{\partial x_2} + e_{31}(x_2)\frac{\partial \phi}{\partial x_2}, \\
\sigma_{22} &= c_{12}(x_2)\frac{\partial u_1}{\partial x_1} + c_{22}(x_2)\frac{\partial u_2}{\partial x_2} + e_{33}(x_2)\frac{\partial \phi}{\partial x_2}, \\
\sigma_{12} &= c_{44}(x_2)(\frac{\partial u_1}{\partial x_2} + \frac{\partial u_2}{\partial x_1}) + e_{15}(x_2)\frac{\partial \phi}{\partial x_1}, \\
D_1 &= e_{15}(x_2)(\frac{\partial u_1}{\partial x_2} + \frac{\partial u_2}{\partial x_1}) - \epsilon_{11}(x_2)\frac{\partial \phi}{\partial x_1}, \\
D_2 &= e_{31}(x_2)\frac{\partial u_1}{\partial x_1} + e_{33}(x_2)\frac{\partial u_2}{\partial x_2} - \epsilon_{33}(x_2)\frac{\partial \phi}{\partial x_2},
\end{aligned} \tag{5}$$

where $c_{ij}(x_2)$, $e_{ij}(x_2)$ and $\epsilon_{ij}(x_2)$ are respectively the elastic moduli, piezoelectric coefficients and dielectric coefficients of the piezoelectric bimaterial defined by

$$\begin{aligned}
&(c_{11}(x_2),\ c_{12}(x_2),\ c_{22}(x_2),\ c_{44}(x_2), \\
&e_{15}(x_2),\ e_{31}(x_2),\ e_{33}(x_2),\ \epsilon_{11}(x_2),\ \epsilon_{33}(x_2)) = \\
&\begin{cases}
(c_{11}^{(1)},\ c_{12}^{(1)},\ c_{22}^{(1)},\ c_{44}^{(1)},\ e_{15}^{(1)},\ e_{31}^{(1)},\ e_{33}^{(1)},\ \epsilon_{11}^{(1)},\ \epsilon_{33}^{(1)}) \\
\qquad \text{for } 0 < x_2 < h, \\
(c_{11}^{(2)},\ c_{12}^{(2)},\ c_{22}^{(2)},\ c_{44}^{(2)},\ e_{15}^{(2)},\ e_{31}^{(2)},\ e_{33}^{(2)},\ \epsilon_{11}^{(2)},\ \epsilon_{33}^{(2)}) \\
\qquad \text{for } x_2 < 0,
\end{cases}
\end{aligned} \tag{6}$$

with $c_{11}^{(p)}$, $c_{12}^{(p)}$, $c_{22}^{(p)}$, $c_{44}^{(p)}$, $e_{15}^{(p)}$, $e_{31}^{(p)}$, $e_{33}^{(p)}$, $\epsilon_{11}^{(p)}$ and $\epsilon_{33}^{(p)}$ $(p = 1, 2)$ being suitable positive constants.

According to the conservation of momentum and the Gauss law of electric flux, the governing partial differential equations for the deformation of the

piezoelectric material are given by

$$\begin{aligned}
c_{11}(x_2)\frac{\partial^2 u_1}{\partial x_1^2} + (c_{12}(x_2) + c_{44}(x_2))\frac{\partial u_2^2}{\partial x_1 \partial x_2} + c_{44}(x_2)\frac{\partial^2 u_1}{\partial x_2^2} \\
+(e_{31}(x_2) + e_{15}(x_2))\frac{\partial \phi^2}{\partial x_1 \partial x_2} = 0, \\
(c_{12}(x_2) + c_{44}(x_2))\frac{\partial u_1^2}{\partial x_1 \partial x_2} + c_{44}(x_2)\frac{\partial^2 u_2}{\partial x_1^2} + c_{22}(x_2)\frac{\partial^2 u_2}{\partial x_2^2} \\
+e_{15}(x_2)\frac{\partial \phi^2}{\partial x_1^2} + e_{33}(x_2)\frac{\partial \phi^2}{\partial x_2^2} = 0, \\
(e_{15}(x_2) + e_{31}(x_2))\frac{\partial u_1^2}{\partial x_1 \partial x_2} + e_{15}(x_2)\frac{\partial^2 u_2}{\partial x_1^2} + e_{33}(x_2)\frac{\partial^2 u_2}{\partial x_2^2} \\
-\epsilon_{11}(x_2)\frac{\partial \phi^2}{\partial x_1^2} - \epsilon_{33}(x_2)\frac{\partial \phi^2}{\partial x_2^2} = 0. \qquad (7)
\end{aligned}$$

Following closely the notation of Barnett and Lothe [4], we introduce the generalized displacements U_J and stresses S_{Ij} as

$$\begin{aligned}
U_J &= \begin{cases} u_j & \text{for } J = j = 1,\ 2, \\ \phi & \text{for } J = 3, \end{cases} \\
S_{Ij} &= \begin{cases} \sigma_{Ij} & \text{for } I = i = 1,\ 2, \\ D_j & \text{for } I = 3, \end{cases}
\end{aligned}$$

and define C_{IjKp} as

$$C_{IjKp} = \begin{cases}
c_{11} & \text{if } (I,j,K,p) = (1,1,1,1), \\
c_{12} & \text{if } (I,j,K,p) = (1,1,2,2) = (2,2,1,1), \\
c_{22} & \text{if } (I,j,K,p) = (2,2,2,2), \\
c_{44} & \text{if } (I,j,K,p) = (1,2,1,2) = (2,1,2,1) = (1,2,2,1) = (2,1,1,2), \\
e_{15} & \text{if } (I,j,K,p) = (2,1,3,1) = (1,2,3,1) = (3,1,2,1) = (3,1,1,2), \\
e_{31} & \text{if } (I,j,K,p) = (1,1,3,2) = (3,2,1,1), \\
e_{33} & \text{if } (I,j,K,p) = (2,2,3,2) = (3,2,2,2), \\
-\epsilon_{11} & \text{if } (I,j,K,p) = (3,1,3,1), \\
-\epsilon_{33} & \text{if } (I,j,K,p) = (3,2,3,2), \\
0 & \text{otherwise,}
\end{cases} \qquad (8)$$

such that (5) and (7) may be rewritten respectively as

$$S_{Ij} = C_{IjKl}\frac{\partial U_K}{\partial x_l} \text{ (for } I = 1, 2, 3;\ j = 1, 2),$$

and

$$C_{IjKl}\frac{\partial^2 U_K}{\partial x_j \partial x_l} = 0 \text{ (for } I = 1, 2, 3). \tag{9}$$

where the Einsteinian convention of summing over repeated indices holds here for the uppercase Latin subscripts which take the values 1, 2 and 3. Note that the coefficients C_{IjKl} are functions of x_2 as defined by (6) for the piezoelectric bimaterial.

Mathematically, the problem stated in Section 2 requires solving (9) subject to suitably prescribed conditions. The conditions on the interface $x_2 = 0$ are given by

$$\left.\begin{array}{c} S_{K2}(x_1, 0^+) = S_{K2}(x_1, 0^-) \\ \Delta U_K(x_1) = 0 \end{array}\right\} \text{ for } (x_1, 0) \text{ on the uncracked parts of the interface,} \tag{10}$$

and by either

$$S_{K2}(x_1, 0^\pm) = -P_K(x_1) \quad \text{for } (x_1, 0) \text{ on electrically impermeable micro-cracks,} \tag{11}$$

or

$$\left.\begin{array}{c} S_{12}(x_1, 0^\pm) = -P_1(x_1) \\ S_{22}(x_1, 0^\pm) = -P_2(x_1) \\ \Delta U_3(x_1) = 0 \end{array}\right\} \text{ for } (x_1, 0) \text{ on electrically permeable micro-cracks,} \tag{12}$$

where $P_1(x_1)$, $P_2(x_1)$ and $P_3(x_1)$ are periodic functions of period L giving the internal loads on the micro-cracks and $\Delta U_K(x_1) = U_K(x_1, 0^+) - U_K(x_1, 0^-)$.

The conditions on the plane $x_2 = h$ (the external edge of the layer) and at the far field are

$$\begin{aligned} S_{K2}(x_1, h) &= 0 \text{ for } -\infty < x_1 < \infty, \\ S_{Kj}(x_1, x_2) &\to 0 \text{ as } x_2 \to -\infty. \end{aligned} \tag{13}$$

3.2 Hypersingular integro-differential equations

For electrically impermeable micro-cracks, the analysis in [23] can be readily employed to formulate the boundary value problems defined by (9), (10), (11) and (13) in terms of a system of the hypersingular integro-differential equations given by

$$\begin{aligned} &\frac{1}{2\pi} \Xint=_0^L U_R(x_1, h)\, \mathrm{Re}\{\sum_{\alpha=1}^{3} G_{RI\alpha}\}[\frac{1}{(x_1 - \xi_1)^2} + \Theta(x_1, \xi_1)]dx_1 \\ &+\frac{1}{2\pi} \int_0^L U_R(x_1, h)\, \mathrm{Re}\{\sum_{\alpha=1}^{3}\sum_{\beta=1}^{3} H_{RI\alpha\beta}\Omega(x_1, \xi_1, \tau_\alpha^{(1)} h - \overline{\tau}_\beta^{(1)} h)\}dx_1 \\ &-\frac{1}{2\pi} \sum_{k=1}^{M} \int_{a^{(k)}}^{b^{(k)}} \Delta U_R(x_1)\, \mathrm{Re}\{\sum_{\alpha=1}^{3} G_{RI\alpha}\Omega(x_1, \xi_1, -\tau_\alpha^{(1)} h)\}dx_1 \\ &-\frac{1}{2\pi} \sum_{k=1}^{M} \int_{a^{(k)}}^{b^{(k)}} \Delta U_R(x_1)\, \mathrm{Re}\{\sum_{\alpha=1}^{3}\sum_{\beta=1}^{3} H_{RI\alpha\beta}\Omega(x_1, \xi_1, -\overline{\tau}_\beta^{(1)} h)\}dx_1 \\ = \;& 0 \quad \text{for } 0 < \xi_1 < L, \end{aligned} \tag{14}$$

and

$$
\begin{aligned}
&-\frac{1}{2\pi}\int_0^L U_R(x_1,h)\,\mathrm{Re}\{\sum_{\alpha=1}^{3}\Omega(x_1,\xi_1,\tau_\alpha^{(1)}h)(G_{RI\alpha}+\sum_{\beta=1}^{3}H_{RI\alpha\beta})\}dx_1\\
&+\frac{1}{2\pi}[\fint_{a^{(k)}}^{b^{(k)}}\frac{\Delta U_R(x_1)\,\mathrm{Re}\{W_{RI}\}}{(x_1-\xi_1)^2}dx_1\\
&+\sum_{\substack{n=1\\n\neq k}}^{M}\int_{a^{(n)}}^{b^{(n)}}\frac{\Delta U_R(x_1)\,\mathrm{Re}\{W_{RI}\}}{(x_1-\xi_1)^2}dx_1\\
&+\sum_{n=1}^{M}\int_{a^{(n)}}^{b^{(n)}}\Delta U_R(x_1)\,\mathrm{Re}\{W_{RI}\}\Theta(x_1,\xi_1)dx_1-\frac{d\Delta U_R(\xi_1)}{d\xi_1}\,\mathrm{Im}\{\pi V_{RI}\}]\\
=\;& P_I(\xi_1)\text{ for }a^{(k)}<\xi_1<b^{(k)}\ (k=1,2,...,M),
\end{aligned}
\tag{15}
$$

where $\fint$ denotes that the integral is to be interpreted in the Hadamard finite-part sense (for details, see Ang [1]), Re denotes the real part of a complex number, the overhead bar denotes the conjugate of a complex number, $G_{RI\alpha}$ and $H_{RI\alpha\beta}$ are constants given by

$$
\begin{aligned}
G_{RI\alpha} &= [L_{R2\alpha}^{(1)}N_{\alpha P}^{(1)}(C_{I2M1}^{(1)}+\tau_\alpha^{(1)}C_{I2M2}^{(1)})]D_{PM}^{(1)},\\
H_{RI\alpha\beta} &= [L_{R2\alpha}^{(1)}Q_{\alpha\beta P}^{(1)}(C_{I2M1}^{(1)}+\overline{\tau}_\beta^{(1)}C_{I2M2}^{(1)})]D_{PM}^{(1)},
\end{aligned}
$$

the constants $Q_{\alpha\beta P}^{(1)}$ are implicitly defined by

$$
\sum_{\alpha=1}^{3}(\overline{A}_{K\alpha}^{(1)}N_{\gamma K}^{(2)}-\overline{L}_{K2\alpha}^{(1)}M_{\gamma K}^{(2)})\overline{Q}_{\alpha\beta P}^{(1)}=(L_{K2\beta}^{(1)}M_{\gamma K}^{(2)}-A_{K\beta}^{(1)}N_{\gamma K}^{(2)})N_{\beta P}^{(1)},
\tag{16}
$$

the constants $L_{I2\alpha}^{(p)}$ $(p=1,\,2)$ are given by

$$
L_{I2\alpha}^{(p)}=(C_{I2K1}^{(p)}+\tau_\alpha^{(p)}C_{I2K2}^{(p)})A_{K\alpha}^{(p)},
\tag{17}
$$

the constants $C_{IjKl}^{(1)}$ and $C_{IjKl}^{(2)}$ denote respectively the material constants C_{IjKl} for the layer and the half-space, the constants $\tau_1^{(p)}$, $\tau_2^{(p)}$ and $\tau_3^{(p)}$ are

the complex numbers with positive imaginary parts and they are solutions of the sextic equations in $\tau^{(p)}$ given by

$$\det \begin{bmatrix} c_{11}^{(p)} + c_{44}^{(p)}(\tau^{(p)})^2 & (c_{12}^{(p)} + c_{44}^{(p)})\tau^{(p)} & (e_{31}^{(p)} + e_{15}^{(p)})\tau^{(p)} \\ (c_{12}^{(p)} + c_{44}^{(p)})\tau^{(p)} & c_{44}^{(p)} + c_{22}^{(p)}(\tau^{(p)})^2 & e_{15}^{(p)} + e_{33}^{(p)}(\tau^{(p)})^2 \\ (e_{31}^{(p)} + e_{15}^{(p)})\tau^{(p)} & e_{15}^{(p)} + e_{33}^{(p)}(\tau^{(p)})^2 & -\epsilon_{11}^{(p)} - \epsilon_{33}^{(p)}(\tau^{(p)})^2 \end{bmatrix} = 0, \quad (18)$$

the constants $A_{K\alpha}^{(p)}$ are chosen to satisfy

$$\begin{bmatrix} c_{11}^{(p)} + c_{44}^{(p)}(\tau_\alpha^{(p)})^2 & (c_{12}^{(p)} + c_{44}^{(p)})\tau_\alpha^{(p)} & (e_{31}^{(p)} + e_{15}^{(p)})\tau_\alpha^{(p)} \\ (c_{12}^{(p)} + c_{44}^{(p)})\tau_\alpha^{(p)} & c_{44}^{(p)} + c_{22}^{(p)}(\tau_\alpha^{(p)})^2 & e_{15}^{(p)} + e_{33}^{(p)}(\tau_\alpha^{(p)})^2 \\ (e_{31}^{(p)} + e_{15}^{(p)})\tau_\alpha^{(p)} & e_{15}^{(p)} + e_{33}^{(p)}(\tau_\alpha^{(p)})^2 & -\epsilon_{11}^{(p)} - \epsilon_{33}^{(p)}(\tau_\alpha^{(p)})^2 \end{bmatrix} \begin{bmatrix} A_{1\alpha}^{(p)} \\ A_{2\alpha}^{(p)} \\ A_{3\alpha}^{(p)} \end{bmatrix} = 0, \quad (19)$$

in which $A_{1\alpha}^{(p)}$ and $A_{2\alpha}^{(p)}$ can be solved by taking $A_{3\alpha}^{(p)} = 1$ (see Athanasius et al. [3]), the matrices $N_{\gamma K}^{(p)}$ and $M_{\gamma K}^{(p)}$ are respectively the inverses of $A_{\gamma K}^{(p)}$ and $L_{R2\alpha}^{(p)}$ and the constants $D_{PM}^{(p)}$ are implicitly defined by

$$\mathrm{Im}\{\sum_{\alpha=1}^{3} L_{I2\alpha}^{(p)} N_{\alpha R}^{(p)}\} D_{RP}^{(p)} = \delta_{IP}, \quad (20)$$

with δ_{IP} being the Kronecker-delta and Im denoting the imaginary parts of a complex number, the constants W_{RI} and V_{RI} are defined by

$$\begin{aligned} W_{RI} &= \sum_{\alpha=1}^{3} G_{RI\alpha} + \sum_{\alpha=1}^{3}\sum_{\beta=1}^{3} H_{RI\alpha\beta}, \\ V_{RI} &= \sum_{\alpha=1}^{3}\sum_{\beta=1}^{3} H_{RI\alpha\beta} - \sum_{\alpha=1}^{3} G_{RI\alpha}, \end{aligned}$$

and the functions $\Theta(x_1, \xi_1)$ and $\Omega(x_1, \xi_1, z)$ are defined as

$$\begin{aligned} \Theta(x_1, \xi_1) &= \frac{1}{L^2}\Psi_1(\frac{L + x_1 - \xi_1}{L}) + \frac{1}{L^2}\Psi_1(\frac{L + \xi_1 - x_1}{L}), \\ \Omega(x_1, \xi_1, z) &= \frac{1}{(x_1 - \xi_1 + z)^2} + \frac{1}{L^2}\Psi_1(\frac{L + x_1 - \xi_1 + z}{L}) \\ &\quad + \frac{1}{L^2}\Psi_1(\frac{L - x_1 + \xi_1 - z}{L}), \end{aligned}$$

with Ψ_1 being the trigamma function. Note that the Greek subscripts α, β and γ have the values 1, 2 and 3.

For electrically permeable micro-cracks, the corresponding hypersingular integro-differential equations for the interfacial conditions in (12) can be obtained from (15) by letting $I = i = 1, 2$ (instead of $I = 1, 2, 3$) and $\Delta U_3(x_1) = 0$. The unknown functions in the hypersingular integro-differential equations are $\Delta U_1(x_1)$ and $\Delta U_2(x_1)$.

3.3 Computational procedure for estimating effective properties

For electrically impermeable micro-cracks, the numerical procedures in Wang et al. [23] can be employed to solve the hypersingular integro-differential equations (14) and (15) for the unknown generalized displacement jumps $\Delta U_R(x_1)$. Three independent sets of electroelastostatic loads denoted by $P_I = P_I^{(q)}$ ($q = 1$, 2 and 3) are applied in (14) and (15) to solve for the corresponding generalized displacement jumps denoted by $\Delta U_R^{(q)}(x_1)$. Once the unknown $\Delta U_R^{(q)}(x_1)$ are obtained, the effective properties $k_{ij}^{(\mathrm{imp})}$, b_i, c_i and w in (3) may be calculated by using

$$\int_0^L \begin{bmatrix} P_1^{(q)}(x_1) \\ P_2^{(q)}(x_1) \\ P_3^{(q)}(x_1) \end{bmatrix} dx_1 = \begin{bmatrix} k_{11}^{(\mathrm{imp})} & k_{12}^{(\mathrm{imp})} & b_1 \\ k_{21}^{(\mathrm{imp})} & k_{22}^{(\mathrm{imp})} & b_2 \\ c_1 & c_2 & w \end{bmatrix} \cdot \sum_{k=1}^{M} \int_{a^{(k)}}^{b^{(k)}} \begin{bmatrix} \Delta U_1^{(q)}(x_1) \\ \Delta U_2^{(q)}(x_1) \\ \Delta U_3^{(q)}(x_1) \end{bmatrix} dx_1,$$
$$\text{for } q = 1,\ 2 \text{ and } 3. \tag{21}$$

For electrically permeable micro-cracks, since $\Delta U_3^{(q)}(x_1) = 0$, only two independent sets of elastostatic loads $P_i^{(q)}$ ($q = 1$, 2) are used to numerically solve the hypersingular integro-differential equations (15) for I having only the values 1 and 2 to obtain the corresponding displacement jumps $\Delta U_R^{(q)}(x_1)$ ($R = 1$, 2). Once the unknown $\Delta U_R^{(q)}(x_1)$ are obtained, the effective proper-

ties $k_{ij}^{(\mathrm{per})}$ in the interfacial conditions in (4) may be calculated by using

$$\begin{aligned} \int_0^L \begin{bmatrix} P_1^{(q)}(x_1) \\ P_2^{(q)}(x_1) \end{bmatrix} dx_1 &= \begin{bmatrix} k_{11}^{(\mathrm{per})} & k_{12}^{(\mathrm{per})} \\ k_{21}^{(\mathrm{per})} & k_{22}^{(\mathrm{per})} \end{bmatrix} \cdot \sum_{k=1}^{M} \int_{a^{(k)}}^{b^{(k)}} \begin{bmatrix} \Delta U_1^{(q)}(x_1) \\ \Delta U_2^{(q)}(x_1) \end{bmatrix} dx_1, \\ \text{for } q &= 1,\ 2. \end{aligned} \tag{22}$$

The statistical approach described in Wang et al. [25] is adopted here for the estimation of the effective properties of the interface. For statistical simulations, random interfaces are created. To form a random interface, the lengths of the M micro-cracks in the region $0 < x_1 < L$, $x_2 = 0$, are randomly generated by using a chi-square distribution $\chi^2(m)$ of degree of freedom m. The micro-cracks are then randomly located in the region $0 < x_1 < L$, $x_2 = 0$.

In reality, the distribution of micro-cracks on an interface tends to skew towards shorter micro-cracks, that is, a realistic interface tends to have more shorter micro-cracks and fewer longer ones. Such a distribution of micro-cracks can be generated by using a lower degree of freedom, such as $m = 5$, in the chi-square distribution. Thus, in all the specific cases studied in Section 4, we use the chi-square distribution $\chi^2(5)$ to generate the lengths of the micro-cracks.

For an electrically impermeable interface having average micro-crack length $\widehat{a}$ and damage ratio ρ defined by

$$\widehat{a} = \frac{1}{M} \sum_{m=1}^{M} (b^{(m)} - a^{(m)}) \text{ and } \rho = \frac{1}{L} \sum_{m=1}^{M} (b^{(m)} - a^{(m)}), \tag{23}$$

we compute the non-dimensionalized effective properties $\widehat{a}k_{ij}^{(\mathrm{imp})}/c_{44}^{(2)}$, $\widehat{a}b_i/\sqrt{c_{44}^{(2)}\epsilon_{11}^{(2)}}$, $\widehat{a}c_i/\sqrt{c_{44}^{(2)}\epsilon_{11}^{(2)}}$ and $\widehat{a}w/(-\epsilon_{11}^{(2)})$ as follows. We generate N random interfaces, all of which have the same respective values for ρ and the relative width $h/\widehat{a}$ of the layer, and we calculate and average up the non-dimensionalized effective properties of all the random interfaces. The average non-dimensionalized

effective properties of all the random interfaces are then the required non-dimensionalized effective properties of the electrically impermeable interface of the electrically impermeable interface for fixed values of ρ and $h/\widehat{a}$.

The non-dimensionalized effective properties $\widehat{a}k_{ij}^{(\mathrm{per})}/c_{44}^{(2)}$ of an electrically permeable interface having average micro-crack length $\widehat{a}$ and damage ratio ρ are computed via statistical simulations in a similar way.

Like in Wang et al. [22, 23, 24, 25], we have investigated here the number of micro-cracks (over a period interval of the interface) required for homogenizing the interface. If the number of micro-cracks needed for homogenizing the interface is M_0 then the average values of the non-dimensionalized effective properties of the random interfaces do not change significantly with M (the number of micro-cracks per period interval of the interface) when M exceeds M_0. Using $N = 50$ (that is, a sample of 50 random interfaces) in a statistical simulation for estimating the effective properties for various values of ρ, $\widehat{a}/h$ and the material constants in the layer and the half-space, we find that the interface can be homogenized by taking $M_0 = 40$.

In the statistical simulations for the case studies in Section 4, we use a sample of 50 random interfaces, each of which contains 40 micro-cracks, to estimate the interfacial effective properties. As mentioned earlier on, the micro-crack length follows the chi-square distribution $\chi^2(5)$.

4 Case studies on the effective stiffness coefficients of the interface

In this section, we conduct parametric studies on the effective properties of micro-damaged interfaces between a piezoelectric layer and a piezoelectric half-space by using the statistical approach outlined in Section 3.3. In all the cases studied below, the effective properties $\widehat{a}k_{ij}^{(\mathrm{per})}/c_{44}^{(2)}$ (for electrically

permeable interfaces) are found to be extremely close to $\widehat{a}k_{ij}^{(\mathrm{imp})}/c_{44}^{(2)}$ (for electrically impermeable interfaces). Thus, only the results for electrically impermeable interfaces are presented here.

4.1 Effects of $\widehat{a}/h$ and ρ on an interface between particular materials

Here we consider the cases where the layer and the interface are occupied by specific piezoelectric materials. The effects of $\widehat{a}/h$ (the average half microcrack length over the width of the layer) and ρ (the damage ratio) on the effective properties of the interface are investigated.

The layer is taken to be occupied by the piezoelectric material PZT ceramic with material constants $c_{11}^{(1)} = 13.8 \times 10^{10}$ N/m^2, $c_{22}^{(1)} = 12.9 \times 10^{10}$ N/m^2, $c_{44}^{(1)} = 2.45 \times 10^{10}$ N/m^2, $c_{12}^{(1)} = 9.39 \times 10^{10}$ N/m^2, $e_{15}^{(1)} = 14.0$ C/m^2, $e_{31}^{(1)} = 1.02$ C/m^2, $e_{33}^{(1)} = 30.7$ C/m^2, $\epsilon_{11}^{(1)} = 151 \times 10^{-10}$ C/(V m) and $\epsilon_{33}^{(1)} = 130 \times 10^{-10}$ C/(V m) (Wang and Noda [26]). The half-space is occupied by the piezoelectric material barium titanate ($BaTiO_3$) with material constants given by $c_{11}^{(2)} = 16.6 \times 10^{10}$ N/m^2, $c_{22}^{(2)} = 16.2 \times 10^{10}$ N/m^2, $c_{44}^{(2)} = 4.3 \times 10^{10}$ N/m^2, $c_{12}^{(2)} = 7.8 \times 10^{10}$ N/m^2, $e_{15}^{(2)} = 11.6$ C/m^2, $e_{31}^{(2)} = -4.4$ C/m^2, $e_{33}^{(2)} = 18.6$ C/m^2, $\epsilon_{11}^{(2)} = 112 \times 10^{-10}$ C/(V m) and $\epsilon_{33}^{(2)} = 126 \times 10^{-10}$ C/(V m) (Wang et al. [27]).

For selected values of ρ, Figures 2, 3, 4 and 5 plot respectively the non-dimensionalized effective properties $\widehat{a}k_{11}^{(\mathrm{imp})}/c_{44}^{(2)}$, $\widehat{a}k_{22}^{(\mathrm{imp})}/c_{44}^{(2)}$, $\widehat{a}b_2/\sqrt{c_{44}^{(2)}\epsilon_{11}^{(2)}}$ and $\widehat{a}w/(-\epsilon_{11}^{(2)})$ against $\widehat{a}/h$. The values of $\widehat{a}k_{12}^{(\mathrm{imp})}/c_{44}^{(2)}$, $\widehat{a}k_{21}^{(\mathrm{imp})}/c_{44}^{(2)}$, $\widehat{a}b_1/\sqrt{c_{44}^{(2)}\epsilon_{11}^{(2)}}$ and $\widehat{a}c_1/\sqrt{c_{44}^{(2)}\epsilon_{11}^{(2)}}$ are observed to be extremely small compared to $\widehat{a}k_{11}^{(\mathrm{imp})}/c_{44}^{(2)}$, $\widehat{a}k_{22}^{(\mathrm{imp})}/c_{44}^{(2)}$, $\widehat{a}b_2/\sqrt{c_{44}^{(2)}\epsilon_{11}^{(2)}}$ and $\widehat{a}w/(-\epsilon_{11}^{(2)})$, having magnitudes in the order of at least 10^{-9}. Also, the value of b_2 is observed to be very close to the value of c_2.

For a fixed ρ, the figures show that the effective properties $\widehat{a}k_{11}^{(\mathrm{imp})}/c_{44}^{(2)}$, $\widehat{a}k_{22}^{(\mathrm{imp})}/c_{44}^{(2)}$, $\widehat{a}b_2/\sqrt{c_{44}^{(2)}\epsilon_{11}^{(2)}}$ and $\widehat{a}w/(-\epsilon_{11}^{(2)})$ decrease as $\widehat{a}/h$ increases. The rate of decrease in $\widehat{a}w/(-\epsilon_{11}^{(2)})$ has the smallest magnitude compared to the corresponding ones in $\widehat{a}k_{11}^{(\mathrm{imp})}/c_{44}^{(2)}$, $\widehat{a}k_{22}^{(\mathrm{imp})}/c_{44}^{(2)}$ and $\widehat{a}b_2/\sqrt{c_{44}^{(2)}\epsilon_{11}^{(2)}}$, that is, the plane edge $x_2 = h$ of the layer apparently has a relatively small influence on the effective property $\widehat{a}w/(-\epsilon_{11}^{(2)})$. The figures also show that all the effective properties for a fixed value of $\widehat{a}/h$ decrease with increasing damage ratio ρ. This observation may be explained as follows. If the micro-cracks occupy a larger area on the interface, they are less stable, giving rise to larger magnitude generalized displacement jumps $\Delta U_J(x_1)$ over the micro-cracks and hence smaller effective properties.

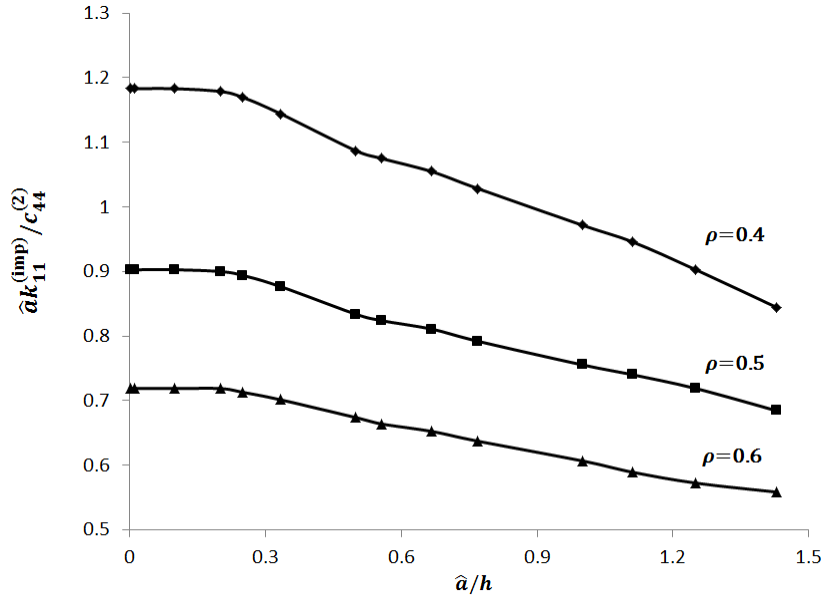

Figure 2. Plots of $\widehat{a}k_{11}^{(\mathrm{imp})}/c_{44}^{(2)}$ against $\widehat{a}/h$ for $\rho = 0.4$, 0.5 and 0.6.

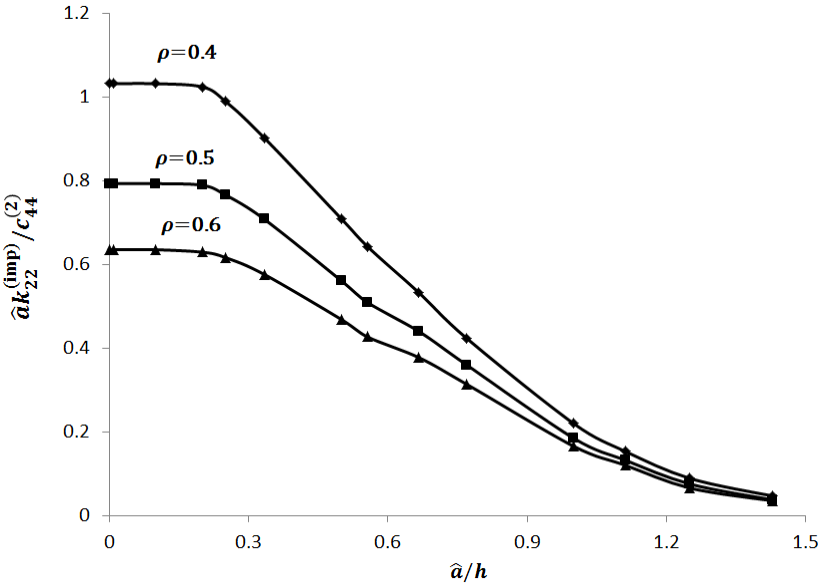

Figure 3. Plots of $\widehat{a}k_{22}^{(\mathrm{imp})}/c_{44}^{(2)}$ against $\widehat{a}/h$ for $\rho = 0.4$, 0.5 and 0.6.

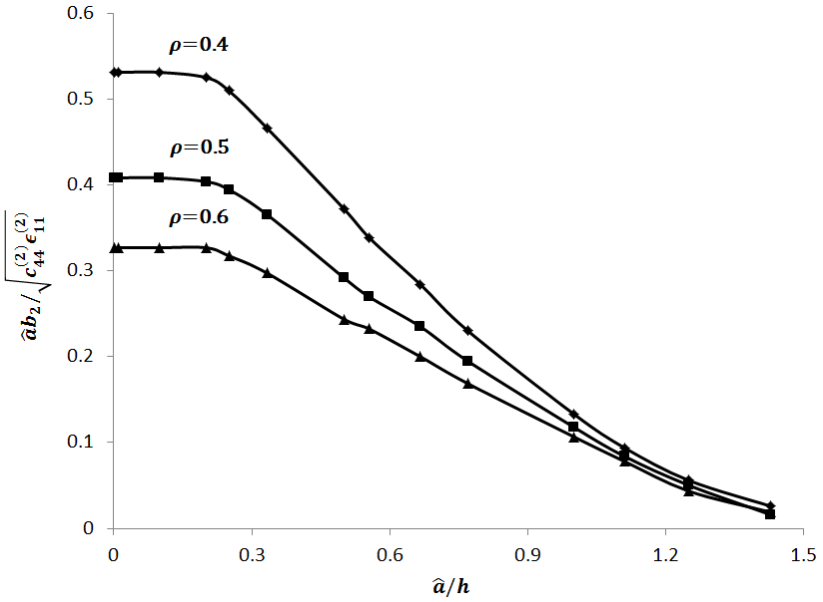

Figure 4. Plots of $\widehat{a}b_2/\sqrt{c_{44}^{(2)}\epsilon_{11}^{(2)}}$ against $\widehat{a}/h$ for $\rho = 0.4$, 0.5 and 0.6.

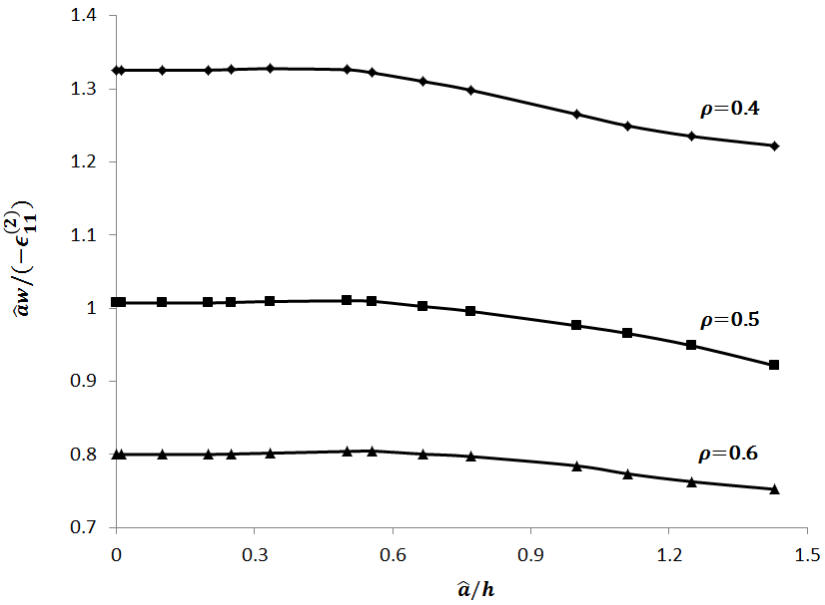

Figure 5. Plots of $\widehat{a}w/(-\epsilon_{11}^{(2)})$ against $\widehat{a}/h$ for $\rho = 0.4$, 0.5 and 0.6.

4.2 Effects of $e_{15}^{(1)}/e_{15}^{(2)}$, $e_{31}^{(1)}/e_{31}^{(2)}$ and $e_{33}^{(1)}/e_{33}^{(2)}$

The effects of the non-dimensionalized piezoelectric coupling coefficients $e_{15}^{(1)}/e_{15}^{(2)}$, $e_{31}^{(1)}/e_{31}^{(2)}$ and $e_{33}^{(1)}/e_{33}^{(2)}$ on the effective properties of the interface are studied here.

As in Section 4.1, the material in the half-space is taken to be $BaTiO_3$. The layer is taken to have the same elastic moduli and the dielectric constants with the half-space, but it has piezoelectric coefficients such that $e_{15}^{(1)}/e_{15}^{(2)} = e_{31}^{(1)}/e_{31}^{(2)} = e_{33}^{(1)}/e_{33}^{(2)} = g$, where g is a non-negative constant.

For $\widehat{a}/h = 0.5$, Figures 6, 7, 8 and 9 plot respectively the non-dimensionalized effective properties $\widehat{a}k_{11}^{(\mathrm{imp})}/c_{44}^{(2)}$, $\widehat{a}k_{22}^{(\mathrm{imp})}/c_{44}^{(2)}$, $\widehat{a}b_2/\sqrt{c_{44}^{(2)}\epsilon_{11}^{(2)}}$ and $\widehat{a}w/(-\epsilon_{11}^{(2)})$ against $\log_{10} g$ for selected values of ρ. Note that the values of $\widehat{a}k_{12}^{(\mathrm{imp})}/c_{44}^{(2)}$,

$\widehat{a}k_{21}^{(\mathrm{imp})}/c_{44}^{(2)}$, $\widehat{a}b_1/\sqrt{c_{44}^{(2)}\epsilon_{11}^{(2)}}$ and $\widehat{a}c_1/\sqrt{c_{44}^{(2)}\epsilon_{11}^{(2)}}$ are observed to be in the order of 10^{-9} or even smaller. As before, b_2 is observed to be very close to c_2.

Figures 6, 7 and 9 show that $\widehat{a}k_{11}^{(\mathrm{imp})}/c_{44}^{(2)}$, $\widehat{a}k_{22}^{(\mathrm{imp})}/c_{44}^{(2)}$ and $\widehat{a}w/(-\epsilon_{11}^{(2)})$ increase with $\log_{10} g$ for $-1 < \log_{10} g < 2$. For $2 < \log_{10} g < 3$, the values of $\widehat{a}k_{11}^{(\mathrm{imp})}/c_{44}^{(2)}$, $\widehat{a}k_{22}^{(\mathrm{imp})}/c_{44}^{(2)}$ and $\widehat{a}w/(-\epsilon_{11}^{(2)})$ do not change very much. As $g \to 0^+$, $\widehat{a}k_{11}^{(\mathrm{imp})}/c_{44}^{(2)}$, $\widehat{a}k_{22}^{(\mathrm{imp})}/c_{44}^{(2)}$ and $\widehat{a}w/(-\epsilon_{11}^{(2)})$ tend to constants.

For a fixed value of ρ, Figure 8 shows that $\widehat{a}b_2/\sqrt{c_{44}^{(2)}\epsilon_{11}^{(2)}}$ has a local maximum at around $g = 10$ and tends to constants as g becomes larger or approaches zero. It is obvious that the values of $\widehat{a}b_2/\sqrt{c_{44}^{(2)}\epsilon_{11}^{(2)}}$ are not equal to zero. This demonstrates that the widely used assumption, which considers the effective properties b_i and c_i as zero, may not be valid.

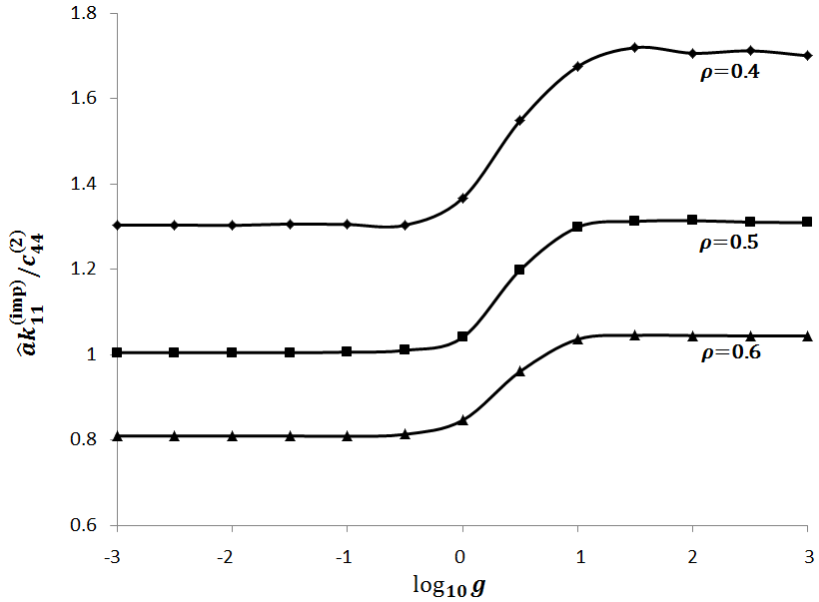

Figure 6. Plots of $\widehat{a}k_{11}^{(\mathrm{imp})}/c_{44}^{(2)}$ against $\log_{10} g$ for $\rho = 0.4$, 0.5 and 0.6 and $\widehat{a}/h = 0.5$.

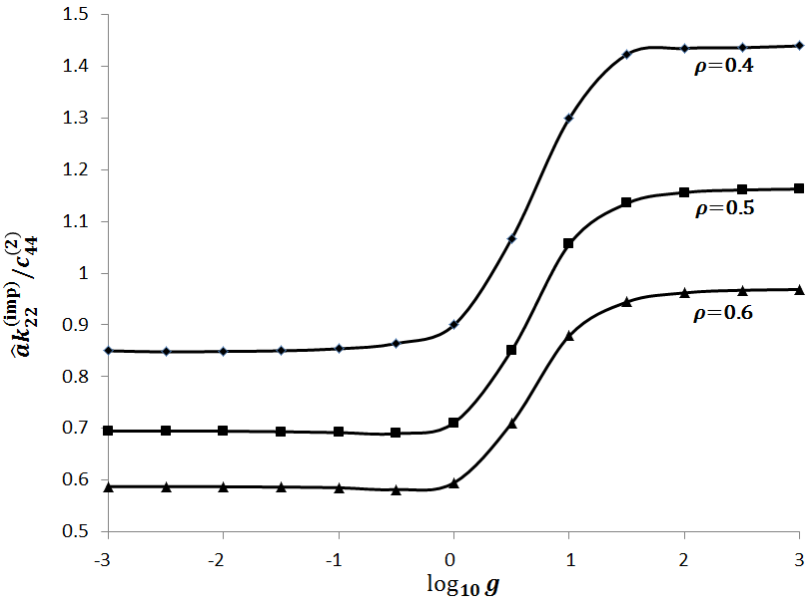

Figure 7. Plots of $\widehat{a}k_{22}^{(\mathrm{imp})}/c_{44}^{(2)}$ against $\log_{10} g$ for $\rho = 0.4$, 0.5 and 0.6 and $\widehat{a}/h = 0.5$.

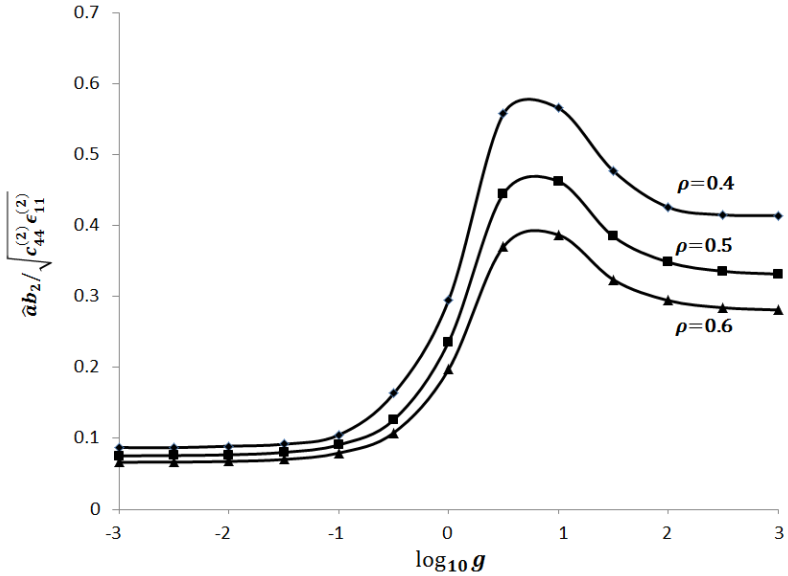

Figure 8. Plots of $\widehat{a}b_2/\sqrt{c_{44}^{(2)}\epsilon_{11}^{(2)}}$ against $\log_{10} g$ for $\rho = 0.4$, 0.5 and 0.6 and $\widehat{a}/h = 0.5$.

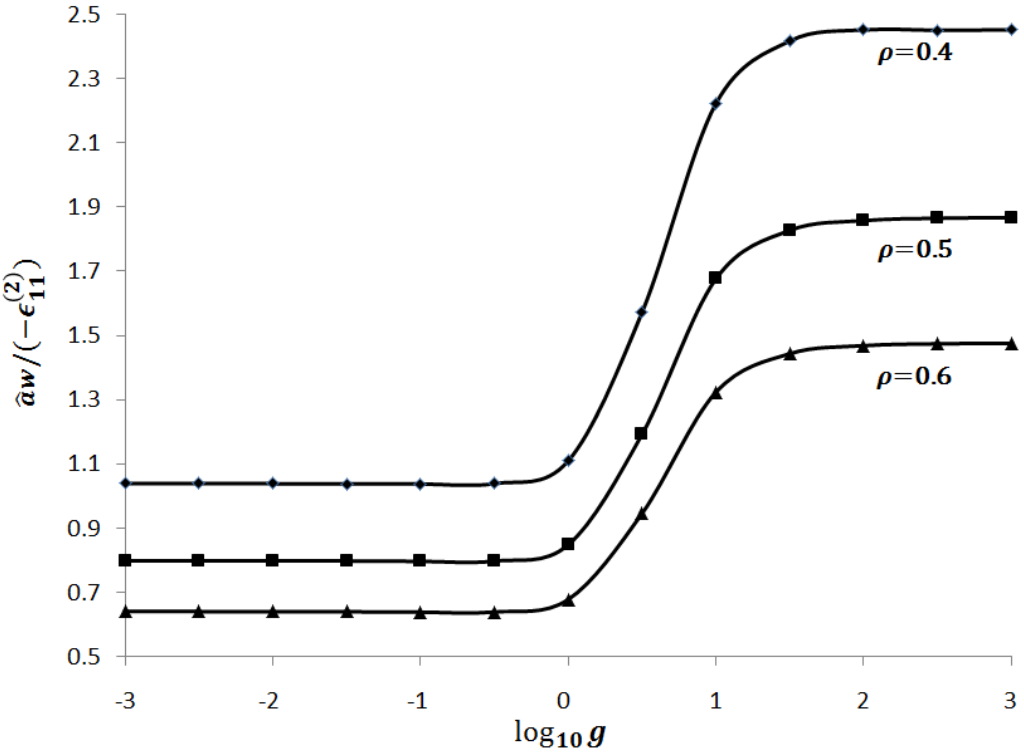

Figure 9. Plots of $\widehat{a}w/(-\epsilon_{11}^{(2)})$ against $\log_{10} g$ for $\rho = 0.4$, 0.5 and 0.6 and $\widehat{a}/h = 0.5$.

For selected values of g, Figures 10, 11, 12 and 13 plot respectively $\widehat{a}k_{11}^{(\mathrm{imp})}/c_{44}^{(2)}$, $\widehat{a}k_{22}^{(\mathrm{imp})}/c_{44}^{(2)}$, $\widehat{a}b_2/\sqrt{c_{44}^{(2)}\epsilon_{11}^{(2)}}$ and $\widehat{a}w/(-\epsilon_{11}^{(2)})$ against $\widehat{a}/h$ for $\rho = 0.5$. For a fixed g, Figures 10, 11 and 12 show that $\widehat{a}k_{11}^{(\mathrm{imp})}/c_{44}^{(2)}$, $\widehat{a}k_{22}^{(\mathrm{imp})}/c_{44}^{(2)}$ and $\widehat{a}b_2/\sqrt{c_{44}^{(2)}\epsilon_{11}^{(2)}}$ decrease with $\widehat{a}/h$. Figure 13 shows that the trend in the variation of $\widehat{a}w/(-\epsilon_{11}^{(2)})$ against $\widehat{a}/h$ may be different depending on the magnitude of g, that is, on the magnitude of the piezoelectric coefficients in the layer. For $g = 5$, it appears that $\widehat{a}w/(-\epsilon_{11}^{(2)})$ increases as $\widehat{a}/h$ increases. However, for the smaller values of g, $\widehat{a}w/(-\epsilon_{11}^{(2)})$ seems to decrease with increasing $\widehat{a}/h$.

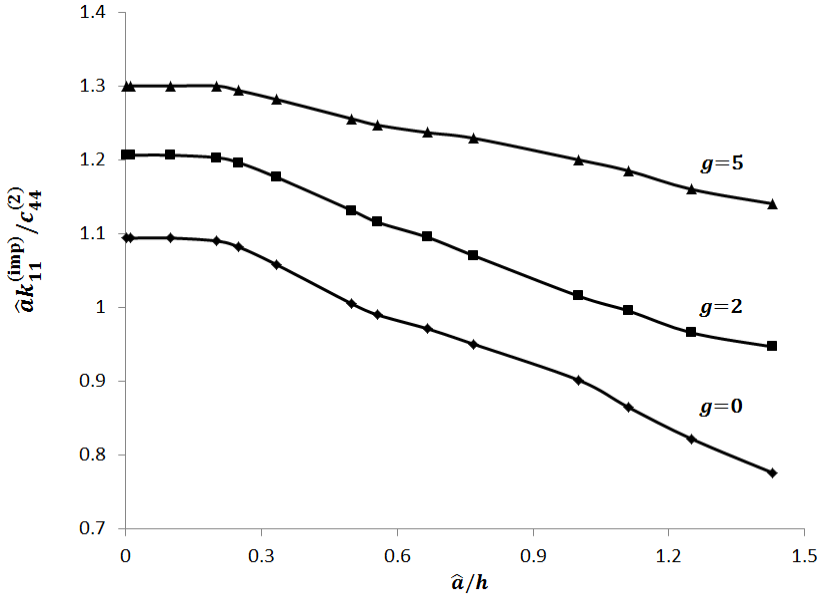

Figure 10. Plots of $\widehat{a}k_{11}^{(\mathrm{imp})}/c_{44}^{(2)}$ against $\widehat{a}/h$ for selected values of g and $\rho = 0.5$.

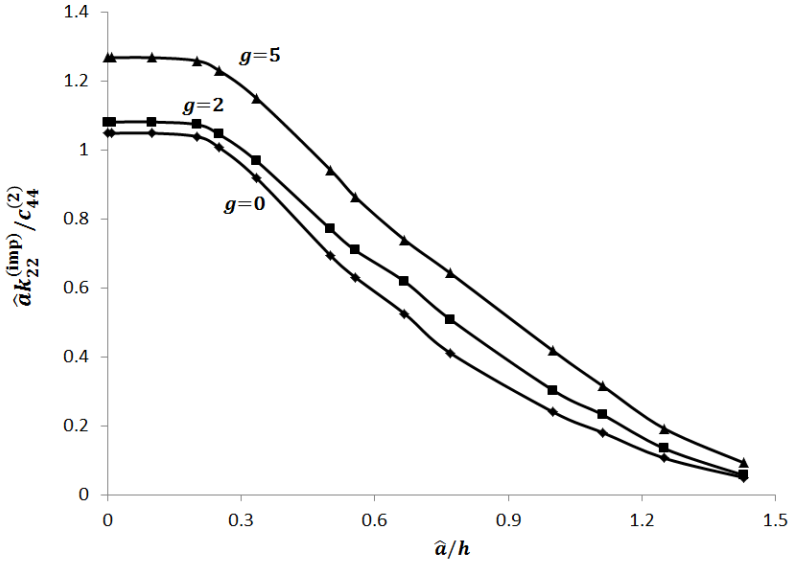

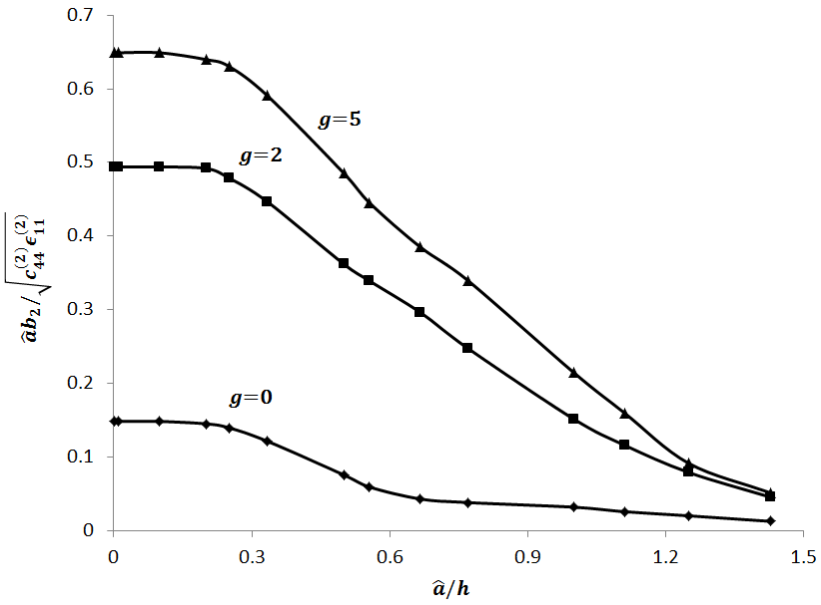

Figure 12. Plots of $\widehat{a}b_2/\sqrt{c_{44}^{(2)}\epsilon_{11}^{(2)}}$ against $\widehat{a}/h$ for selected values of g and $\rho = 0.5$.

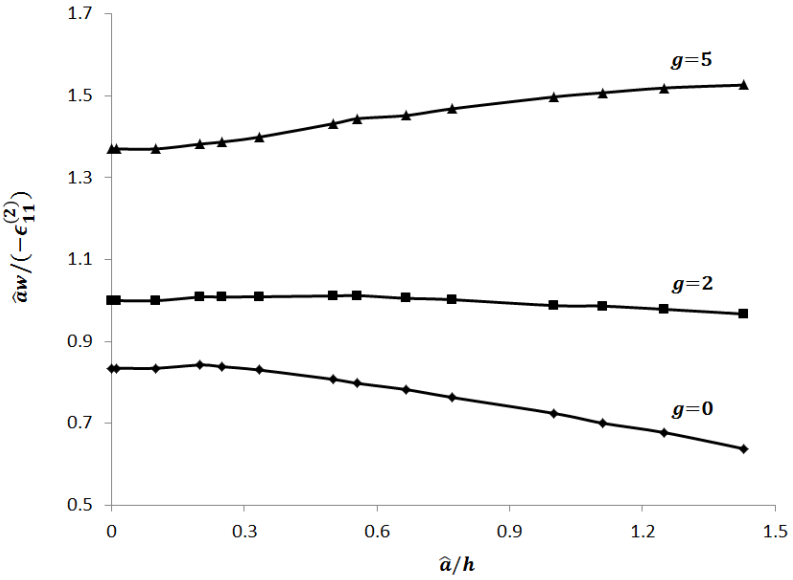

Figure 13. Plots of $\widehat{a}w/(-\epsilon_{11}^{(2)})$ against $\widehat{a}/h$ for selected values of g and $\rho = 0.5$.

4.3 Effects of $c_{11}^{(1)}/c_{11}^{(2)}$, $c_{12}^{(1)}/c_{12}^{(2)}$, $c_{22}^{(1)}/c_{22}^{(2)}$ and $c_{44}^{(1)}/c_{44}^{(2)}$

In this subsection, we study how varying the relative strength $c_{11}^{(1)}/c_{11}^{(2)}$, $c_{12}^{(1)}/c_{12}^{(2)}$, $c_{22}^{(1)}/c_{22}^{(2)}$ and $c_{44}^{(1)}/c_{44}^{(2)}$ of the material in the layer may affect the effective properties of the interface.

Again, take the half-space to be occupied by $BaTiO_3$. The dielectric constants and the piezoelectric coefficients in the layer are taken to have the same values with those in the half-space, but the elastic moduli in the layer are taken to be given by $c_{11}^{(1)}/c_{11}^{(2)} = c_{12}^{(1)}/c_{12}^{(2)} = c_{22}^{(1)}/c_{22}^{(2)} = c_{44}^{(1)}/c_{44}^{(2)} = \beta$ (where β is a positive constant).

For $\widehat{a}/h = 0.5$, Figures 14, 15, 16 and 17 plot respectively the effective properties $\widehat{a}k_{11}^{(\mathrm{imp})}/c_{44}^{(2)}$, $\widehat{a}k_{22}^{(\mathrm{imp})}/c_{44}^{(2)}$, $\widehat{a}b_2/\sqrt{c_{44}^{(2)}\epsilon_{11}^{(2)}}$ and $\widehat{a}w/(-\epsilon_{11}^{(2)})$ against $\log_{10}\beta$ for selected values of ρ. As before, the values of $\widehat{a}k_{12}^{(\mathrm{imp})}/c_{44}^{(2)}$, $\widehat{a}k_{21}^{(\mathrm{imp})}/c_{44}^{(2)}$,

$\widehat{a}b_1/\sqrt{c_{44}^{(2)}\epsilon_{11}^{(2)}}$ and $\widehat{a}c_1/\sqrt{c_{44}^{(2)}\epsilon_{11}^{(2)}}$ are observed to be in the order of 10^{-9} or even smaller and b_2 is observed to be very close to c_2.

For a fixed ρ, we observe that $\widehat{a}k_{11}^{(\mathrm{imp})}/c_{44}^{(2)}$, $\widehat{a}k_{22}^{(\mathrm{imp})}/c_{44}^{(2)}$ and $\widehat{a}b_2/\sqrt{c_{44}^{(2)}\epsilon_{11}^{(2)}}$ increase significantly, but $\widehat{a}w/(-\epsilon_{11}^{(2)})$ decreases, as β increases, that is, as the elastic moduli in the layer are getting larger compared to the elastic moduli in the half-space. It appears that increasing the elastic moduli in the layer has a more drastic influence on $\widehat{a}k_{11}^{(\mathrm{imp})}/c_{44}^{(2)}$ and $\widehat{a}k_{22}^{(\mathrm{imp})}/c_{44}^{(2)}$ than $\widehat{a}b_2/\sqrt{c_{44}^{(2)}\epsilon_{11}^{(2)}}$ and $\widehat{a}w/\sqrt{c_{44}^{(2)}\epsilon_{11}^{(2)}}$. As the layer becomes extremely soft, $\widehat{a}k_{11}^{(\mathrm{imp})}/c_{44}^{(2)}$, $\widehat{a}k_{22}^{(\mathrm{imp})}/c_{44}^{(2)}$ and $\widehat{a}b_2/\sqrt{c_{44}^{(2)}\epsilon_{11}^{(2)}}$ tend to zero and $\widehat{a}w/(-\epsilon_{11}^{(2)})$ tends to a non-zero constant.

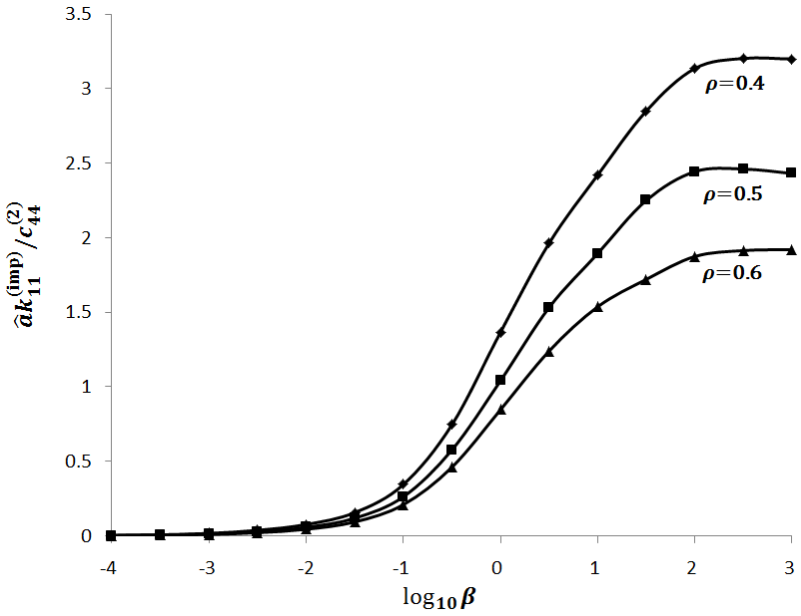

Figure 14. Plots of $\widehat{a}k_{11}^{(\mathrm{imp})}/c_{44}^{(2)}$ against $\log_{10}\beta$ for selected values of ρ and $\widehat{a}/h = 0.5$.

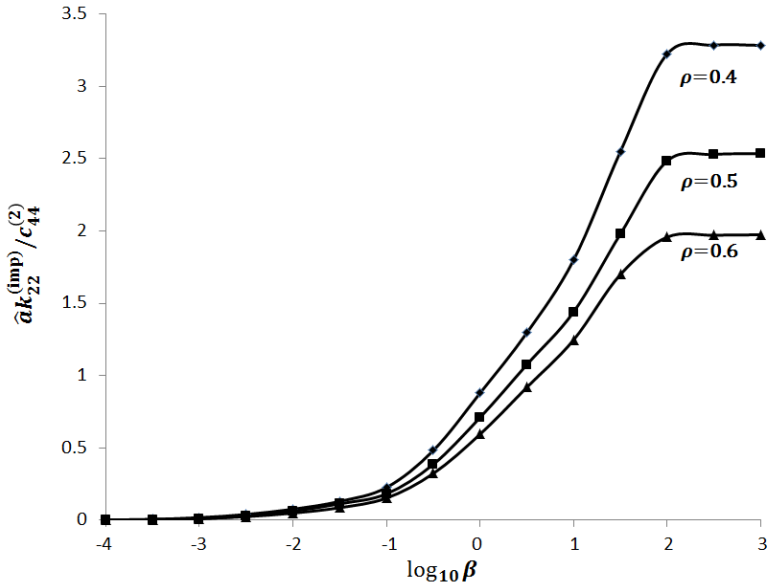

Figure 15. Plots of $\widehat{a}k_{22}^{(\mathrm{imp})}/c_{44}^{(2)}$ against $\log_{10}\beta$ for selected values of ρ and $\widehat{a}/h = 0.5$.

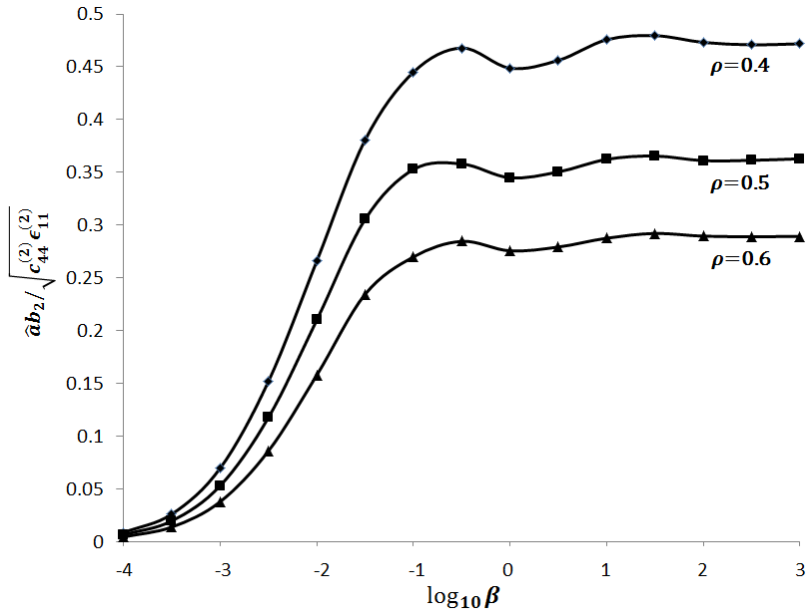

Figure 16. Plots of $\widehat{a}b_2/\sqrt{c_{44}^{(2)}\epsilon_{11}^{(2)}}$ against $\log_{10}\beta$ for selected values of ρ and $\widehat{a}/h = 0.5$.

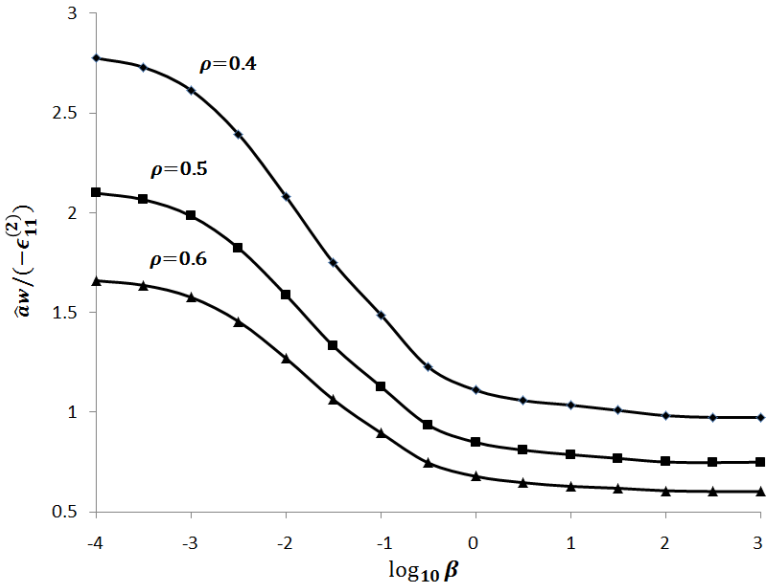

Figure 17. Plots of $\widehat{a}w/(-\epsilon_{11}^{(2)})$ against $\log_{10}\beta$ for selected values of ρ and $\widehat{a}/h = 0.5$.

4.4 Effects of $\epsilon_{11}^{(1)}/\epsilon_{11}^{(2)}$ and $\epsilon_{33}^{(1)}/\epsilon_{33}^{(2)}$

Here the effects of the non-dimensionalized dielectric constants $\epsilon_{11}^{(1)}/\epsilon_{11}^{(2)}$ and $\epsilon_{33}^{(1)}/\epsilon_{33}^{(2)}$ on the effective properties of the interface are investigated.

The half-space is still taken to be occupied by $BaTiO_3$. The elastic moduli and the piezoelectric coefficients in the layer are taken to have the same values with the ones in the layer, but the dielectric constants in the layer are given by $\epsilon_{11}^{(1)}/\epsilon_{11}^{(2)} = \epsilon_{33}^{(1)}/\epsilon_{33}^{(2)} = \gamma$ (where γ is a positive constant).

For $\widehat{a}/h = 0.5$ and selected values of ρ, the effective properties $\widehat{a}k_{11}^{(\mathrm{imp})}/c_{44}^{(2)}$, $\widehat{a}k_{22}^{(\mathrm{imp})}/c_{44}^{(2)}$, $\widehat{a}b_2/\sqrt{c_{44}^{(2)}\epsilon_{11}^{(2)}}$ and $\widehat{a}w/(-\epsilon_{11}^{(2)})$ are plotted against $\log_{10}\gamma$ in Figures 18, 19, 20 and 21 respectively. As before, the values of $\widehat{a}k_{12}^{(\mathrm{imp})}/c_{44}^{(2)}$, $\widehat{a}k_{21}^{(\mathrm{imp})}/c_{44}^{(2)}$, $\widehat{a}b_1/\sqrt{c_{44}^{(2)}\epsilon_{11}^{(2)}}$ and $\widehat{a}c_1/\sqrt{c_{44}^{(2)}\epsilon_{11}^{(2)}}$ are observed to be negligible and the difference between b_2 and c_2 is insignificant.

From the figures, $\widehat{a}k_{11}^{(\mathrm{imp})}/c_{44}^{(2)}$, $\widehat{a}k_{22}^{(\mathrm{imp})}/c_{44}^{(2)}$ and $\widehat{a}b_2/\sqrt{c_{44}^{(2)}\epsilon_{11}^{(2)}}$ decrease in magnitude as the ratio γ increases (that is, as the dielectric constants in the layer are larger than those in the half-space), while the magnitude of $\widehat{a}w/(-\epsilon_{11}^{(2)})$ increases with increasing γ. As γ increases, $\widehat{a}k_{11}^{(\mathrm{imp})}/c_{44}^{(2)}$, $\widehat{a}k_{22}^{(\mathrm{imp})}/c_{44}^{(2)}$ and $\widehat{a}b_2/\sqrt{c_{44}^{(2)}\epsilon_{11}^{(2)}}$ decrease at a rate much smaller than that at which $\widehat{a}w/(-\epsilon_{11}^{(2)})$ increases, that is, varying the dielectric constants in the layer appears to have a greater influence on $\widehat{a}w/(-\epsilon_{11}^{(2)})$ than the other effective properties of the interface.

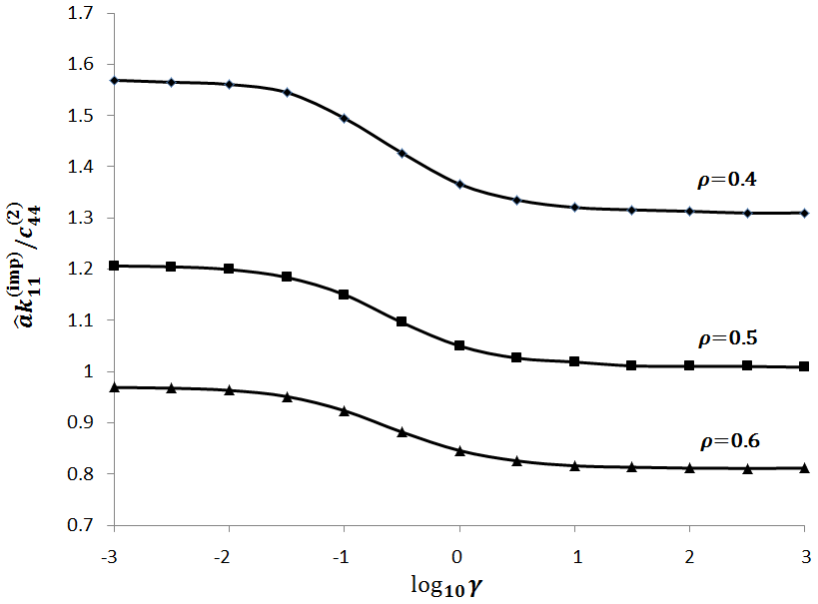

Figure 18. Plots of $\widehat{a}k_{11}^{(\mathrm{imp})}/c_{44}^{(2)}$ against $\log_{10}\gamma$ for selected values of ρ and $\widehat{a}/h = 0.5$.

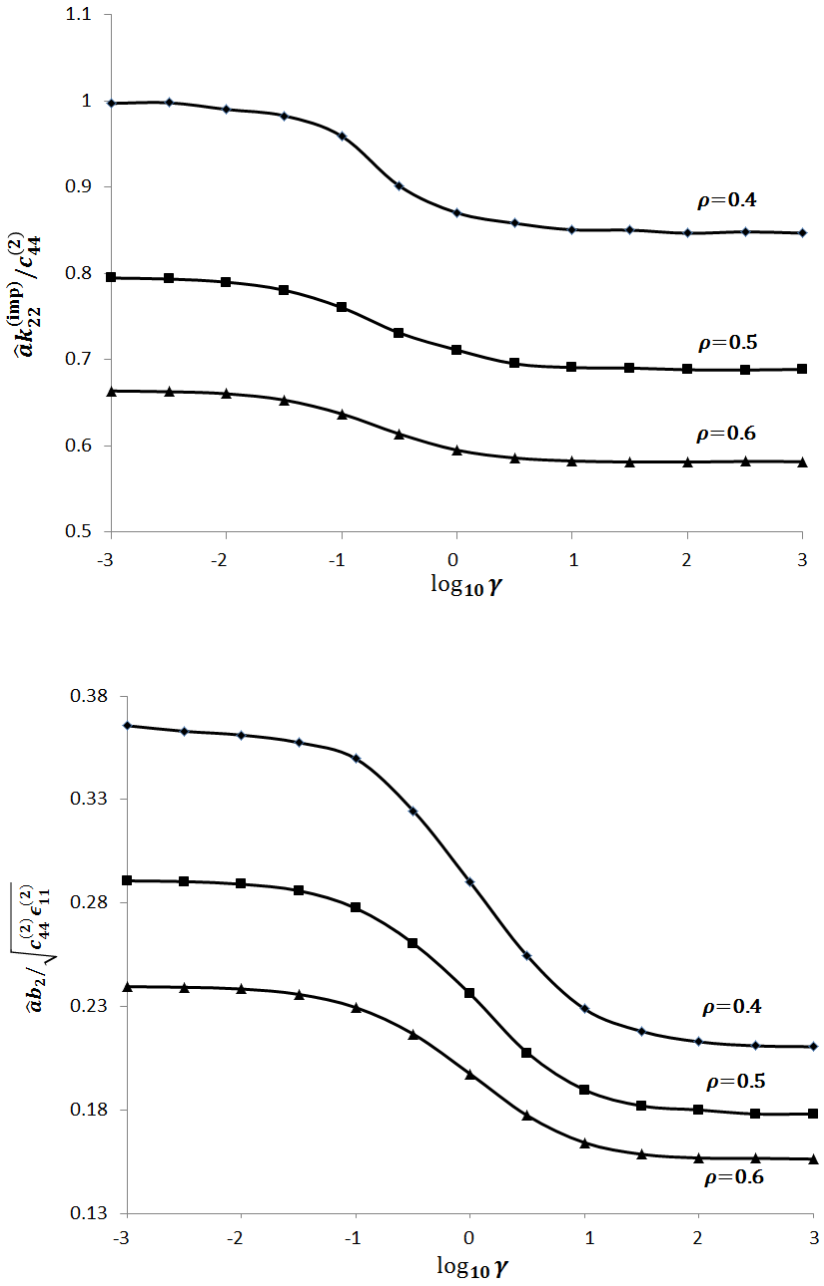

Figure 20. Plots of $\widehat{a}b_2/\sqrt{c_{44}^{(2)}\epsilon_{11}^{(2)}}$ against $\log_{10}\gamma$ for selected values of ρ and $\widehat{a}/h = 0.5$.

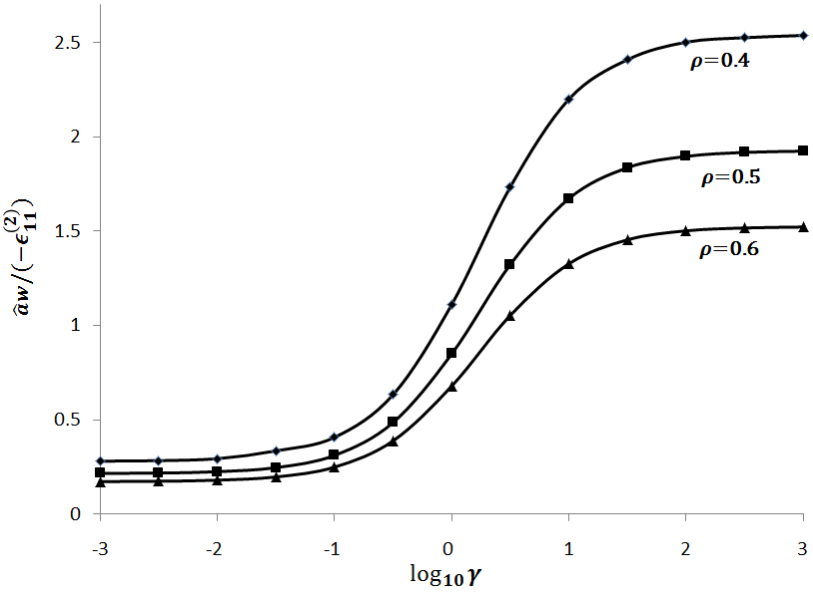

Figure 21. Plots of $\widehat{a}w/(-\epsilon_{11}^{(2)})$ against $\log_{10}\gamma$ for selected values of ρ and $\widehat{a}/h = 0.5$.

5 Summary and conclusions

A micro-statistical model is used to analyze the effective properties of a micro-damaged interface between a piezoelectric layer and a piezoelectric half-space under inplane electroelastostatic deformations. The interface is modeled as damaged by periodic arrays of electrically permeable or impermeable micro-cracks. The boundary conditions on the interfacial micro-cracks give rise to hypersingular integro-differential equations with the displacement jumps and electrical potential jump across the interface being unknown functions to be determined. For a given interface, once the hypersingular integro-differential equations are solved for a set of independent loads on the micro-cracks, the effective properties of the interface can be readily computed. For a statistical

approach, the effective properties are estimated from the mean values of a sample of interfaces containing a sufficient number of micro-cracks that have randomly generated lengths and positions over a period interval of the interface.

As in (3) and (4), the effective properties of interest here are characterized by the parameters $k_{ij}^{(\mathrm{imp})}$, b_i, c_i and w for electrically impermeable interfaces and by $k_{ij}^{(\mathrm{per})}$ for electrically permeable interfaces. From numerous case studies involving a wide range of values for the damage ratio, the average half length of the micro-cracks over the thickness of the layer and the material constants in the layer and the half-space, we find that there is no significant difference between $k_{ij}^{(\mathrm{imp})}$ and $k_{ij}^{(\mathrm{per})}$.

Furthermore, the effective properties $k_{12}^{(\mathrm{imp})}$, $k_{21}^{(\mathrm{imp})}$, b_1 and c_1 are found to be extremely small compared to $k_{11}^{(\mathrm{imp})}$, $k_{22}^{(\mathrm{imp})}$, b_2, c_2 and w. The values of b_2 and c_2 are only very small for cases where the layer is extremely soft compared to the half-space. They are not equal to zero in general. Thus, the rather widely used assumption in which b_i and c_i are taken to be zero may be called into question.

To gain further useful physical insights into the behaviors of the imperfect interface, we have examined in detail how the material constants, the damage ratio of the interface and the width of the layer affect the effective properties of the interface. The results obtained appear to be intuitively and qualitatively acceptable.

Acknowledgment

The authors would like to acknowledge the support from the Singapore Ministry of Education Tier 1 Research Grant No. 81/15 awarded by Nanyang

Technological University.

References

[1] W. T. Ang, *Hypersingular Integral Equations in Fracture Analysis,* Woodhead Publishing, Cambridge, 2013.

[2] W. T. Ang, X. Wang and H. Fan, Effective behavior of a microscopically damaged interface between a layer and a half-space occupied by dissimilar piezoelectric media under antiplane deformations, *International Journal of Solids and Structures* **96** (2016)1-10.

[3] L. Athanasius, W. T. Ang and I. Sridhar, Electro-elastostatic analysis of multiple cracks in an infinitely long piezoelectric strip: a hypersingular integral approach, *European Journal of Mechanics-A/Solids* **29** (2010) 410-419.

[4] D. M. Barnett and J. Lothe, Dislocations and line charges in anisotropic piezoelectric insulators, *Physica Status Solidi (b)* **67** (1975) 105-111.

[5] Y. Benveniste and T. Miloh, Imperfect soft and stiff interfaces in two-dimensional elasticity, *Mechanics of Materials* **33** (2001) 309-323.

[6] W. Q. Chen and K. Y. Lee, Exact solution of angle-ply piezoelectric laminates in cylindrical bending with interfacial imperfections, *Composite Structures* **65** (2004) 329-337.

[7] H. Fan and K. Y. Sze, A micro-mechanics model for imperfect interface in dielectric materials, *Mechanics of Materials* **33** (2001) 363-370.

[8] H. Fan, J. S. Yang and L. M. Xu, Piezoelectric waves near an imperfectly bonded interface between two half-spaces, *Applied Physics Letter* **88** (2006) 203509.

[9] Z. Hashin, The spherical inclusion with imperfect interface, *ASME Journal of Applied Mechanics* **58** (1991) 444-449.

[10] J. P. Jones and J. S. Whittier, Waves at a flexibly bonded interface, *Journal of Applied Mechanics* **34** (1967) 905-909.

[11] H. Y. Kuo, Effective property of multiferroic fibrous composites with imperfect interfaces, *Smart Materials and Structures* **22** (2013) 105005.

[12] Y. D. Li and K. Y. Lee, Effect of an imperfect interface on the SH wave propagating in a cylindrical piezoelectric sensor, *Ultrasonics* **50** (2010) 473-478.

[13] Y. D. Li, T. Xiong and L. H. Dong, A new interfacial imperfection coupling model (IICM) and its effect on the facture behavior of a layered multiferroic composite: Anti-plane case, *European Journal of Mechanics A/Solids* **52** (2015) 26-36.

[14] Y. D. Li, T. Xiong and L. H. Dong, Interfacial imperfection coupling model with application to the in-plane fracture problem of a multiferroic composite, *International Journal of Solids and Structures* **54** (2015) 31-41.

[15] K. I. Park, J. H. Son, G. T. Hwang, C. K. Jeong, J. Ryu, M. Koo, I Choi, S. H. Lee, M. Byun, Z. L. Wang and K. J. Lee, Highly-efficient, flexible piezoelectric PZT thin film nanogenerator on plastic substrates, *Advanced materials* **26** (2014) 2514-2520.

[16] K. I. Park, S. Xu, Y. Liu, G. T. Hwang, S. J. Kang, Z. L. Wang and K. J. Lee, Piezoelectric $BaTiO_3$ thin film nanogenerator on plastic substrates, *Nano Letters* **10** (2010) 4939-4943.

[17] Y. Shi, Y. Wan and Z. Zhong, Variational bounds for the effective electroelastic moduli of piezoelectric composites with electromechanical coupling spring-type interfaces, *Mechanics of Materials* **72** (2014) 72-93.

[18] H. M. Shodja, S. M. Tabatabaei and M. T. Kamali, A piezoelectric-inhomogeneity system with imperfect interface, *International journal of engineering science* **44** (2006) 291-311.

[19] H. M. Shodja, S. M. Tabatabaei and M. T. Kamali, A piezoelectric medium containing a cylindrical inhomogeneity: Role of electric capacitors and mechanical imperfections, *International Journal of Solids and Structures* **44** (2007) 6361-6381.

[20] W. H. Sun, G. L. Ju, J. W. Pan and Y. D. Lee, Effects of the imperfect interface and piezoelectric/piezomagnetic stiffening on the SH wave in a multiferroic composite, *Ultrasonics* **51** (2011) 831-838.

[21] S. Trolier-McKinstry and P. Muralt, Thin film piezoelectrics for MEMS, *Journal of Electroceramics* **12** (2004) 7-17.

[22] X. Wang, W. T. Ang and H. Fan, A micromechanical-statistical model based on hypersingular boundary integral equations for analyzing a pair of parallel interfaces weakened by antiplane micro-cracks, *Computers and Structures* **157** (2015) 178-188.

[23] X. Wang, W. T. Ang and H. Fan, Hypersingular integral and integro-differential micromechanical models for an imperfect interface between a

thin orthotropic layer and an orthotropic half-space under inplane elastostatic deformations, *Engineering Analysis with Boundary Elements* **52** (2015) 32-43.

[24] X. Wang, W. T. Ang and H. Fan, Hypersingular integral equation based micromechanical models for a microscopically damaged antiplane interface between a thin elastic layer and an elastic half space, *Applied Mathematical Modelling* **39** (2015) 6501–6516.

[25] X. Wang, H. Fan and W. T. Ang, On micromechanical-statistical modeling of microscopically damaged interfaces under antiplane deformations, *International Journal of Solids and Structures* **51** (2014) 2327-2335.

[26] B. L. Wang and N. Noda, Crack initiation in PZT-4 piezoelectric ceramic strip, *Journal of Theoretical and Applied Fracture Mechanics* **33** (2000) 35-47.

[27] Y. Wang, Y. Su, J. Li and G. J. Weng, A theory of magnetoelectric coupling with interface effects and aspect-ratio dependence in piezoelectric-piezomagnetic composites, *Journal of Applied Physics* **117** (2015) 164106.

[28] Y. Y. Zhou, W. Q. Chen and C. F. Lü, Semi-analytical solution for orthotropic piezoelectric laminates in cylindrical bending with interfacial imperfections, *Composite Structures* **92** (2010) 1009-1018.